PHOTONIC STRUCTURES BASED ON SLOT WAVEGUIDES FOR NANOSENSORS: STATE OF THE ART AND FUTURE DEVELOPMENTS

**Vittorio M. N. Passaro, Mario La Notte, Benedetto Troia, Lorenzo Passaquindici,
Francesco De Leonardis & Giovanni Giannoccaro**

Photonics Research Group, Dipartimento di Elettrotecnica ed Elettronica, Politecnico di Bari,
via Edoardo Orabona n. 4, 70125 Bari, Italy
E-mail: passaro@deemail.poliba.it; URL: http://dee.poliba.it/photonicsgroup

ABSTRACT

This review presents the state-of-the-art of Bio-Chemical nanosensors based on silicon Photonics. SOI (Silicon on Insulator) technology offers a number of guiding structures such as slot, rib, strip and silicon wire waveguides. We discuss many sensing principles employed in optical detection, such as absorbance, reflectance, fluorescence, chemiluminescence, bioluminescence and refractive index (RI) measurement. The integration of ultra high sensitive photonic waveguides in interferometer architectures (e.g. Mach Zehnder interferometer) and resonant architectures (e.g. ring resonator, Fabry Perot cavity), allow the detection of ultra low traces of chemical/biochemical analytes and gases. Sensing performance of photonic nanosensors based on silicon Photonics are very attractive, exhibiting ultra high sensitivity and low limit of detection (i.e. pg/mL, pmol/L). Intensive research in this field is motivated by broad applications of photonic sensors in healthcare, environmental monitoring, homeland security, food industry, pharmaceuticals, which require sensitive and rapid analytical tools.

Keywords: *Photonic Nanosensors, Slot Waveguides, Silicon Photonics, Microring Resonators, Bio-Chemical Sensors, Directional Couplers, Cantilever Based Sensors, Disk Resonators, DNA molecules, Lab-on-Chip.*

1. SLOT WAVEGUIDE BASED BIO-CHEMICAL PHOTONIC NANOSENSORS

One of the most important goals of all scientific and industry research efforts is without any doubt the healthcare improvement. In recent years, the ever increasing demand of rapid and effective diagnosis, treatment, and prevention of disease, illness, injury, and other physical impairments in humans, have led to explore different approaches with respect to conventional ones.

In this context, the so called Point-of-Care Tests (POCTs) are defined as any medical test close to the patient [1], which means that it can be found at the hospital, doctor's office or patient's home. This last possibility led by POCTs, enables the patient to avoid hospital appointments, waiting lists and so on. Obviously an efficient POCT needs to be portable, user friendly, cost effective and possibly able to provide to the user a simple interpretation of the measure result. Such requirements perfectly match with actual Lab-On-Chip (LOC) technology.

Taking advantage by both light-matter interaction and electronic signal elaboration capability, Lab-On-Chip is effectively an autonomous and miniaturized microfluidic laboratory. Microfluidics deals with behavior, precise control and manipulation of fluids that are geometrically constrained to a small, typically sub-millimeter, integration scale [2]. The term "micro" stands for small fluid volumes (nl, pl, fl), small size, low energy consumption and micro domain. Another important aspect dealing with LOCs, is the possibility to perform several different analysis on the same chip and at the same time (which is sometimes also more important). By this way, Lab-on-Chip POTCs are expected to invade the market in the next few years.

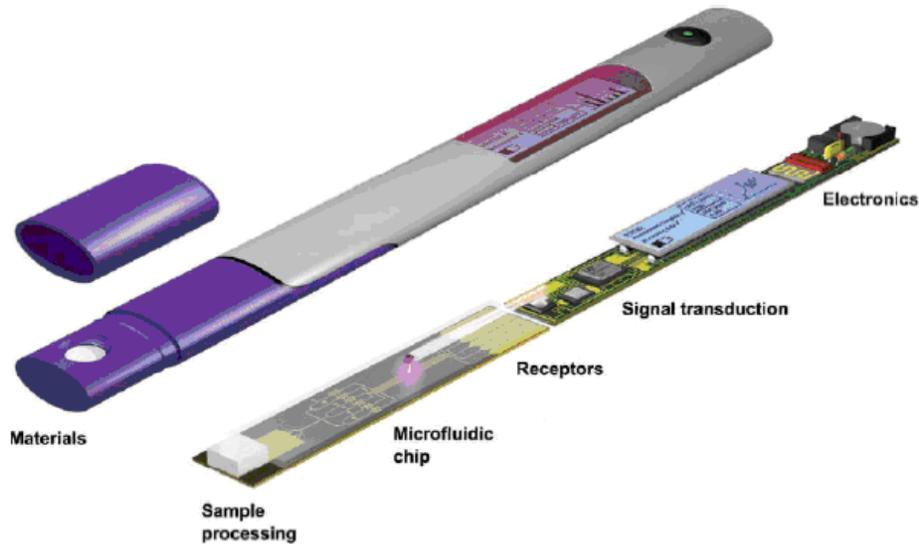A basic example of Lab-on-Chip POCT is shown in Fig. 1.

Figure 1. Example of POCT by IBM Corporation [2].

The device can be schematically divided in several distinguished sections. The first one is a disposable section, provided by a loading port for the liquid sample. Such a part is included into a "reader", which is not disposable and collects all the "intelligence" of the device. The reader contains a unit for sample preparation and processing, a micro-fluidic network for splitting, moving and mixing sample and reagent, a sensor (which can use receptors for labeled or label free detection), a transducer (to convert the information generated by the sensor in an electrical signal), the electronics for signal processing and, finally, a user interface unit for results visualization.

Chemical and bio-chemical sensors, including DNA, proteins, antigens and cells nanosensors, can be classified with respect to their sensing principle, such as absorbance [3], reflectance [4], fluorescence [5], chemiluminescence [6], bioluminescence [7], or refractive index (RI) measurements [8], to name a few. Another kind of classification deals with labeling method. In fact, bio-sensors can be broadly divided into two categories: label-based and label-free sensors. Label based-sensors can be defined as devices that use biological or chemical receptors to detect analytes (molecules) in a sample, to provide information on the binding. Fluorescence is by far the most used labeling method, in which target molecules are tagged with fluorescent dyes and the fluorescence spectrum is detected in the presence of the targeted molecules. This allows for extremely sensitive detection down to the single-molecule level. However, quantitative measurements are difficult to be achieved, the process is laborious, and the tags may affect the function of the bio-molecules.

In contrast, label-free sensors detect targeted molecules in their natural form by attaching those molecules to probe molecules on the surface of the sensor and measuring the change in the physical properties of the sensor (surface sensing), or simply measuring the change of the properties of the sensor due to the change of the refractive index of the medium (homogeneous sensing).

Among all bio-sensors developed and proposed in the last few years, photonics ones have reached a lot of interest in both scientific and enterprise world. In fact, nowadays Photonics is considered one of the most promising technology platforms for the realization of micro- and nano-systems, able to make a great leap forward in improving our living conditions and health. The great technological improvements due to micro and nano-electronics, have led to an enormous development of photonics sensors, as demonstrated by the large amount of proposed devices. Ring resonators, surface plasmonics and fiber-optic-based sensors have been proposed and demonstrated over the last few years [9,10,11]. In particular, great efforts have been made in the field of silicon photonics, which can be considered, by now, a stand-alone research field. CMOS-compatibility and availability of a great amount of devices (sources, modulators, passive waveguides, switches, etc.) make Silicon Photonics the best solution in order to fabricate compact, efficient and low cost micro and nanoscale devices, simultaneously achieving high integration capabilities with CMOS electronics.

With reference to photonic sensors, the sensing element is typically an optical waveguide, and the sensitive property is represented by the effective index of the optical mode propagating into the structure. In Silicon On Insulator (SOI) technology, optical waveguides are realized on wafers composed by a top silicon layer, typically a few hundreds of

nanometers thick, a buried oxide (BOX) substrate, 1-2 μm-thick and a bottom silicon layer (several hundreds of μm-thick) which serves as mechanical support for the optical chip. This solution allows to obtain a very high refractive index contrast (~2 @ λ=1.55 μm), being the refractive index of silicon n_{Si}=3.476 @ λ=1.55 μm, and the refractive index of BOX n_{Ox}=1.444 @ λ=1.55 μm. The cover medium (cladding) varies depending on the specific application. It could be typically an aqueous solution, in which the analyte is dissolved (Fig. 2), or simply air.
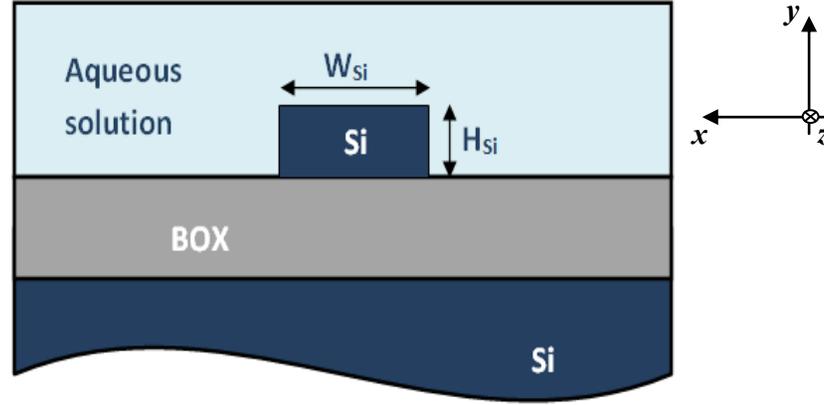

Figure 2. Example of SOI photonic wire waveguide based bio-sensor.

When light propagates into an optical waveguide, a certain amount of power, carried by the optical mode, travels into the core, while the remaining part is confined in cladding and substrate regions. The optical field changes its effective refractive index depending on the concentration of the specific substance, however such a change is related to the percentage of field interacting with the analyte, and so to the confinement factor in the medium containing the analyte. The above mentioned sensing mechanisms (i.e. homogeneous and surface sensing) have been analyzed in detail for optical guided-wave sensors [12].

Homogeneous sensing is very useful to detect a wide variety of gases and chemical species. In order to detect, for example, glucose or ethanol, the optical waveguide is covered by aqueous solution (n_c=1.33 @ λ=1.55 μm), in which the analyte is dissolved. The waveguide sensitivity can be evaluated as [12]:

$$S_h = \left.\frac{\partial n_{eff}}{\partial n_c}\right|_{n_c=n_c^0} = \frac{2n_c^0}{Z_0 P}\iint_C \left|\vec{E}(x,y)\right|^2 dxdy = \frac{2n_c^0\iint_\infty \left|\vec{E}(x,y)\right|^2 dxdy}{Z_0 P}\Gamma_c^I \tag{1}$$

where

$$P = \iint_\infty \left[\left(\bar{E}\times\bar{H}^* + \bar{E}^*\times\bar{H}\right)\cdot\bar{z}\right]dxdy \tag{2}$$

In equation (1), Z_0 is the free space impedance, n_{eff} is the effective mode index, n_c is the solution refractive index, n_c^0 is the solution refractive index in absence of the analyte, $\bar{E}$ and $\bar{H}$ are the electric and magnetic field vector, respectively and Γ_c^I is the optical field intensity confinement factor in the cladding region, defined as follows:

$$\Gamma_c^I = \frac{\iint_C \left|\vec{E}(x,y)\right|^2 dxdy}{\iint_\infty \left|\vec{E}(x,y)\right|^2 dxdy} \tag{3}$$

The integration domain indices, i.e. C and ∞, stands for cladding cross section and whole computational region, respectively.

Differently from homogeneous sensing, surface sensing is based on the immobilization of a very thin layer of receptor molecules on the waveguide surface. Such a layer interacts with the analyte, producing an increase of the molecular adsorbed layer (adlayer) thickness. According with variational theorem, the effective mode index will change as [12]:

$$\Delta n_{eff} = \frac{n_m^2 - \left(n_c^0\right)^2}{Z_0 P} \iint_\Sigma \left|\vec{E}(x, y)\right|^2 dxdy \tag{4}$$

where n_m is the refractive index of the molecular adlayer and Σ represents the surface covered by the adlayer. Similarly to the definition of sensitivity given for homogeneous sensing, it is possible to define the surface waveguide sensitivity as [12]:

$$S_s = \left.\frac{\partial n_{eff}}{\partial \rho}\right|_{n_c = n_c^0} \tag{5}$$

where ρ is the thickness of the molecular adlayer. In this work, we will assume S as homogeneous sensitivity, unless otherwise specified.

Several kinds of waveguides can be realized in SOI technology. Rib, strip and silicon wire waveguides have been extensively studied in the last years. To give an example, Fig. 3 shows the TE-like and TM-like power distributions on the cross section of a single-mode photonic wire waveguide, with $H = 220$ nm and $W = 510$ nm.
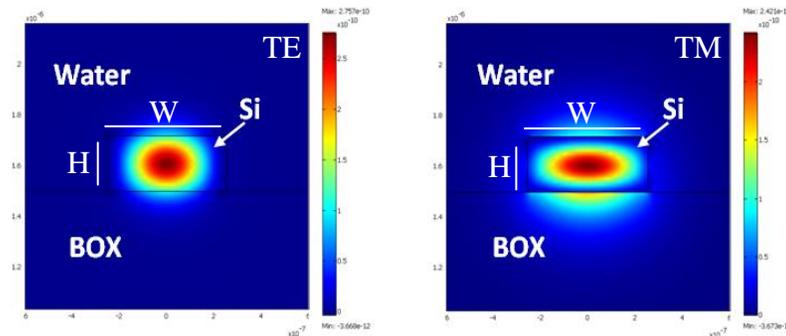

Figure 3. Power distribution on the cross section of a typical single-mode, photonic wire waveguide (H = 220 nm, W = 510 nm) for TE-like (on the left) and TM-like (on the right) polarizations.

It is evident that such a waveguide exhibits a very high power confinement factor in the silicon core for TE-like polarization, involving a very low interaction between the optical field and the possible chemical substance to be detected. A better interaction can be achieved exciting the TM-like polarization, whose major electric field component (E_y) exhibits a discontinuity at the interface between the waveguide top and the cover medium, so the field in the sensitive area is enhanced according to equation (6) below:

$$\left|\frac{E_L}{E_H}\right| = \left(\frac{n_H}{n_L}\right)^2 \tag{6}$$

In equation (6), E_L is the E_y-field component just above the top of the silicon waveguide (i.e. in the low index, cover region), E_H is the E_y-field component just below the top of the silicon waveguide (i.e. in the high index, core region), n_L is the cladding refractive index and n_H is the refractive index of the silicon waveguide core ($n_H = n_{Si} = 3.476$ @ $\lambda = 1.55$ μm). These qualitative considerations are confirmed by the optical intensity confinement factor in the cladding medium, which is $\left(\Gamma_c^I\right)^{TE} = 10.33$ % for TE-like polarization and $\left(\Gamma_c^I\right)^{TM} = 24.32$ % for TM-like polarization. Accordingly to equation (1), the homogeneous sensitivity achieved with such a waveguide is $S_h = 0.14$

for TE-like mode and $S_h = 0.50$ for TM-like mode. This means that, even in the best case of TM-like polarization, a change of the cladding refractive index Δn_c induced by a well defined concentration of a particular analyte will cause a change of the mode effective index, of an half of Δn_c.

A very promising solution, in order to achieve ultra-high sensitivity waveguides, is represented by slot guided-wave structures, whose basic geometry is sketched in Fig. 4.
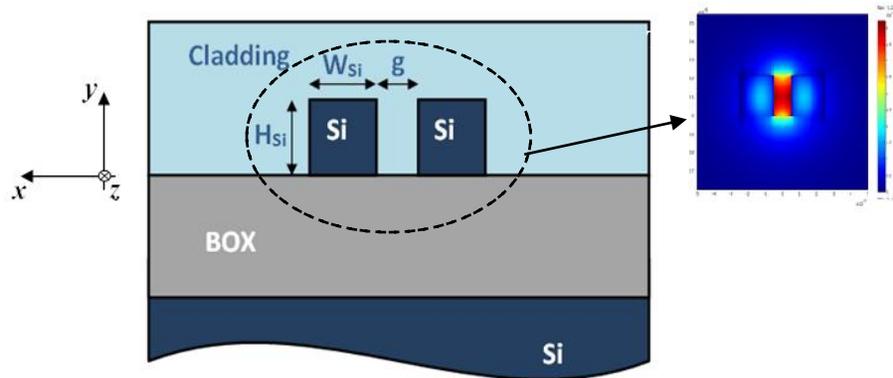

Figure 4. SOI slot waveguide cross section and power spatial distribution for TE-like fundamental mode.

Differently from conventional rib, strip and photonic wire waveguides, slot waveguides are able to confine light into a low index region (cladding), simultaneously preserving an optical guiding nature [12,13]. In fact, while the operative guiding mechanism still remains the total internal reflection (TIR) into the high index medium (silicon wires), slot waveguide takes advantage by the discontinuity of the electric field normal component (E_x) with respect to the boundary surface between high and low refractive index media, according to equation (6). Although the field exponentially decreases in the cladding region, if the gap between silicon wires (g) is sufficiently small (~100-200 nm), the optical intensity in the slot region can be very high. By this way, such a waveguide is very attractive for sensing purposes [14-24], since it enables a very high interaction between light and particles to be detected. Slot waveguide based microring resonators [14-16,19-23,25] and directional couplers [16,26] have been recently proposed and demonstrated, using different kinds of material systems, namely Si_3N_4/SiO_2 [14,19,25,27,28], Si/SiO_2 [15,17,20-24,29], TiO_2/SiO_2 [30], polymers [31,32] and group IV material systems (e.g. SiGeSn, GeC, SiGeC, GeSn) [33,34].

2. MICRORING RESONATOR BASED SENSORS
Microring resonator based sensors use a wavelength interrogation scheme, which is very useful for simultaneously reducing noise and enhancing sensitivity [35]. A microring resonator sensor consists of a waveguide closed into a loop (ring) and one or two input/output bus waveguides, coupled to the ring as sketched in Fig. 5.
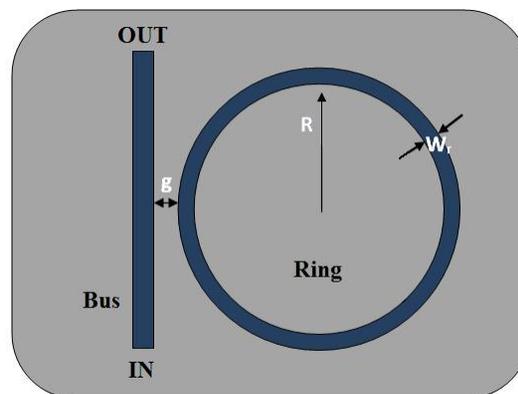

Figure 5. Photonic sensor based on ring resonator coupled to one bus waveguide for I/O signal propagation.

A comprehensive analysis of such a guiding structure involves, even in 2D case, a challenging numerical solution [36]. However, a simpler analysis based on the resonance theory still enables to understand the sensor behavior. The propagation of stationary modes into the ring waveguide only happens for those solutions of Maxwell equations satisfying the well known resonance condition:

$$2\pi R n_{eff} = m\lambda \tag{7}$$

where n_{eff} is the modal effective index, R is the ring resonator radius, m is an integer number (i.e. the resonant order) and λ is the resonant wavelength, able to propagate in the resonant cavity. Equation (7) simply states that a constructive interference at each round trip in the resonator is reached when the optical path length traveled by light is an integer multiple of its wavelength. By this way, only those wavelengths satisfying equation (7), will add constructively in the cavity, involving, after a few round trips, the light extinction at the output port of the bus waveguide, as shown in Fig. 5. The well known transmission function, characterizing the resonant architecture previously shown, is given by [25]:

$$T_{ring}(\lambda) = \frac{\alpha^2 + r^2 - 2\alpha r \cos\left(\dfrac{2\pi L n_{eff}}{\lambda}\right)}{1 + \alpha^2 r^2 - 2\alpha r \cos\left(\dfrac{2\pi L n_{eff}}{\lambda}\right)} \tag{8}$$

In equation (8), r is the coupling coefficient between bus and ring, α is the loss coefficient of the cavity and L is the ring resonator total path length, equal to $2\pi R$. When a specific analyte or gas is concentrated in the cladding medium, the effective index of the propagating mode will change. Such a variation induces a shift of the resonant wavelength, so a new definition of sensitivity can be given [37]:

$$S_\lambda = \left.\frac{\partial\lambda}{\partial n_c}\right|_{n_c = n_c^0} = \frac{\partial\lambda}{\partial n_{eff}}\frac{\partial n_{eff}}{\partial n_c} = \frac{\lambda}{n_g}S \tag{9}$$

In equation (9), S is the waveguide sensitivity (i.e. homogeneous sensitivity S_h), n_g is the group index which takes into account the wavelength dispersion of n_{eff} according to the following equation:

$$n_g = n_{eff} - \lambda\frac{\partial n_{eff}}{\partial\lambda} \tag{10}$$

An important figure of merit that characterizes a photonic sensor is the limit of detection (LOD). It represents the lowest quantity or concentration of a component that can be reliably detected with a given level of confidence. Referring to chemical and bio-chemical sensors, LOD is the lowest detectable concentration of the chemical/biochemical test sample to be monitored and revealed. Obviously, an analytical definition of LOD will depend on both sensor overall architecture and transduction principle performance. Anyways, it can be generically defined as the ratio σ/S_λ, where σ is the noise in the transduction signal and S_λ is the overall sensitivity. Moreover, a generic definition, suitable for optical chemical detection, can be reviewed as follows:

$$LOD = \frac{\Delta\lambda}{S_\lambda} \tag{11}$$

In equation (11), $\Delta\lambda$ is the spectral resolution of OSA (optical spectrum analyzer) to be employed in the experimental setup and S_λ is the overall sensitivity characterizing the photonic sensor. A wavelength resolution of 80 pm is standard in ordinary OSA.

Barrios et al. first have demonstrated a Si_3N_4/SiO_2 slot waveguide based bio-chemical sensor [25,37], using a wavelength interrogation scheme for the optical readout. The proposed device is composed by a single straight

waveguide (bus) coupled with a resonator. Both input/output bus and ring resonator are slot waveguides, as sketched in Fig. 6.
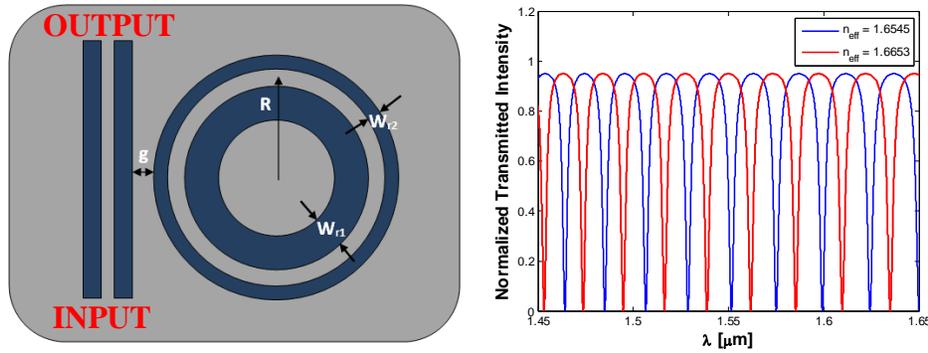

Figure 6. Scheme of SOI slot waveguide based bio-sensor (left), and corresponding normalized transmitted intensity @ λ = 1.3 μm (right).

The device operates at an operative wavelength of 1.3 μm (O-band telecomm applications), where water exhibits a lower absorption coefficient with respect to $\lambda = 1.55$ μm. Both homogeneous and surface sensing have been demonstrated with the proposed device. Si_3N_4 has a lower refractive index ($n_{Si3N4} \sim 2$) with respect to silicon at the operative wavelength $\lambda = 1.3$ μm, allowing a relaxation of requested gap dimension in order to maintain the single mode operation [25]. Furthermore, referring to homogeneous sensing, a wider gap dimension ($g \sim 200$ nm [25]) facilitates a complete slot filling by liquid solutions. The proposed device is characterized by a ring radius $R = 70$ μm, while the thickness of the Si_3N_4 waveguides is set to 300 nm. The transmission spectrum of the sensor has been measured by varying the ethanol concentration in the aqueous solution. Depending on that, the cladding refractive index (n_c) has been found to range between 1.33 and 1.42 and a homogeneous sensitivity $S_\lambda = 212$ nm/RIU (refractive index unit) has been demonstrated, being more than twice larger than that reported for strip waveguides [27], in good agreement with theoretical predictions. The proposed sensor exhibits a LOD as low as 2×10^{-4} RIU.

The same architecture sketched in Fig. 6, has been demonstrated to exhibit high performance even for surface sensing, as reported in [27]. In this work authors demonstrate that bovine serum albumin (BSA) protein and anti-BSA molecular binding reactions can be effectively detected by a label-free slot-waveguide ring resonator, adopting surface sensing. Although the sensor chip is almost identical to that reported in [39], several additional technological steps have to be performed in order to functionalize the sensor surface. After a proper cleaning treatment, for removing organic material and native oxide from sensor surface, the chip has been immersed into aqueous glutaraldehyde (5%) to allow selective, covalent immobilization of anti-BSA antibodies to the Si_3N_4 sensor surface through the formation of imine bonds. After an incubation time into an aqueous solution of anti-BSA and other few chemical treatments, the device has been optically characterized. With such a procedure the sensor surface is functionalized, and immobilized molecules becomes able to capture, in a selective way, the target molecules. Reported experimental measures show that a red shift ($\delta\lambda$) of the resonance wavelength occurs for increasing anti-BSA concentrations. However, a saturation condition is reached for antibodies concentration of 17.2 μg/mL, due to the complete coverage of the sensing surface. The sensor overall surface sensitivity can be defined as [27] $S_{s,\lambda} = \delta\lambda/\sigma_p$, where σ_p represents the surface density of a monolayer of the molecular species to be detected, while LOD can be calculated by equation (11). The biosensor exhibited sensitivities of 1.8 and 3.2 nm/(ng/mm^2) for the detection of anti-BSA and BSA, respectively, while calculated detection limits are 28 and 16 pg/mm^2 for anti-BSA and BSA, respectively.

A very critical aspect concerning photonic bio-sensing is the temperature control. In fact, depending on the material system used for the sensor device, the thermo-optic effect can considerably affect the final measurements. Thermo-optic coefficients (K) for typical material systems used in slot waveguide sensors are in the range 10^{-5}-10^{-4} RIU/K [19], so a very accurate control ($\sim$10-100 mK) is needed to ensure high performance. The temperature effect consists in modal effective index perturbation due to the bulk refractive index change with temperature variations. As a consequence, the effective refractive index shift can be written as:

$$\Delta n_{eff} = \Delta n_{eff}^{SENSING} + \Delta n_{eff}^{TEMPERATURE} \tag{12}$$

Since sensor sensitivity is strictly related to Δn_{eff}, according to equations (1),(5),(9), the resonant wavelength shift will be clearly affected by temperature variations, involving a wrong measure of the parameter to be detected. The final result is a corrupted measure of biological analytes and molecules of interest. Three are the most common approaches used for temperature influence reduction: active temperature control, a-thermal waveguide design, and temperature drift compensation by on chip referencing. The first approach ensures a very high temperature control (~10 mK [19]), however it inevitably increases both size and cost of the optical chip. The second approach deals with a proper design of the sensor geometry, balancing the optical mode power percentage in each material in order to minimize the temperature effect. Such an approach can be very promising due to the different sign of the thermo-optic coefficient of photonic wires, substrate (Si, SiO_2 and Si_3N_4 with $K > 0$) and aqueous solution (water has $K < 0$), and it has been successfully applied in the design of a SOI slot waveguide based ring resonator filter, covered by a polymer material [38]. An extremely low temperature dependence of -2 pm/K has been reported. Finally, the compensation by on chip referencing has been successfully adopted [19]. In this work, a low temperature dependence of -16.6 pm/K has been demonstrated, for a Si_3N_4/SiO_2 slot waveguide ring resonator sensor array, simultaneously showing a very high sensitivity as $S_\lambda = 240$ nm/RIU. Furthermore, a differential temperature sensitivity of only 0.3 pm/K has been reached, by using an on-chip temperature referencing without any individual sensor calibration. Such a result is very promising for highly parallel chemical assays purpose, enabling good sensor-to-sensor repeatability. A detection limit of 8.8×10^{-6} RIU has been experimentally demonstrated in a temperature range of 7 K, without any external temperature control.

Furthermore, using temperature drift compensation by on chip referencing, a packaged optical Si_3N_4/SiO_2 slot-waveguide ring resonator sensor array for multiplex label-free assays in lab-on-chips, has been fabricated and proposed [14]. In this work design, fabrication, and characterization of an array of optical slot waveguide ring resonator sensors, integrated with microfluidic sample handling in a compact cartridge, has been presented. Such a sensor enables multiplexed, real-time, label-free bio-sensing, also providing reference channels for temperature drift compensation and control experiments. The sensor cartridge consists of four, permanently bounded layers, bounded on an alignment platform. Starting from the bottom of the device, there are the optical chip, the fluidics layer, an adhesive film and the hard plastic shell. A *via* is realized in all the three upper layers to enable light coupling to the optical chip. Coupling mechanism is reached by a grating coupler [39], used to couple light coming from an optical fiber into the input optical waveguide. Such a solution allows high coupling efficiency, simultaneously exhibiting large coupling angle tolerance. The optical chip is sketched in Fig. 7 below.
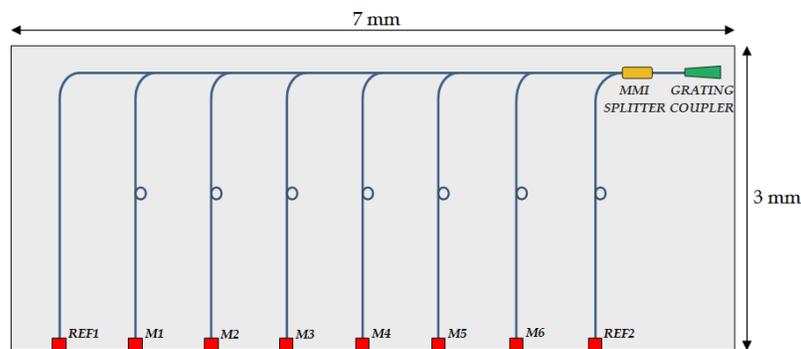

Figure 7. Sketch of Si_3N_4/SiO_2 slot-waveguide ring resonator sensor array [14].

Light coupled into the optical chip is split by a Multi Mode Interference (MMI) into eight identical waveguides. Six of them (namely M1, M2,..., M6) are sensing channels, the channel named REF1 (without any ring resonator) is used for alignment and laser amplitude compensation, while the channel named REF2 acts as a reference for temperature compensation, being covered by SiO_2 layer. The signals coming from the eight channels finally are properly driven to the photodiode array (red squares in Fig. 7). Two cartridges of the proposed device have been tested. The first cartridge has been used for homogeneous sensing, with parallel analysis of both ethanol and methanol. The measured sensitivity has been found to be $S_\lambda = 246$ nm/RIU for both solutions, demonstrating the high repeatability of sensor performance. Furthermore, a detection limit as low as 5×10^{-6} RIU has been estimated. The second cartridge has been tested for surface sensing of several concentrations of anti-BSA. In this case waveguide surface has been previously functionalized by a layer of the molecular linker glutaraldehyde.

Experimental measures have shown a mass surface sensitivity of 1.3 nm/(ng·mm^2), while the estimated detection limit has been found to be 0.9 pg/mm^2.

Moreover, homogeneous sensitivity of Si_3N_4/SiO_2 triple-slot based sensors has been estimated to be improved by 20%, compared to that of a single-slot waveguide [16], as a consequence of a larger localization of the propagating optical mode E-field in the sensing region. On the other hand, multiple-slot waveguides are inevitably more highly affected by scattering losses induced by surface roughness, so degrading the sensor performance.

An important aspect to be considered, when slot bio-sensors are used, deals with optofluidic device reconfigurability. In fact, wetting forces inside the slot channel could be able to trap small amounts of organic liquid [40], which has a damaging effect on sensor performance. Thermal or chemical approaches have been proposed to clean the slot region after each sensor usage, in a Si_3N_4/SiO_2 slot-waveguide based sensor [40].

Till now only Si_3N_4/SiO_2 based slot waveguide sensors have been reviewed. However, the use of SOI technology enables to reach higher index difference than that achievable by Si_3N_4/SiO_2 technology, involving both ultra high sensitivity and low LOD. The main drawback of Si/SiO_2 material system use is essentially the increase of scattering losses induced by sidewalls surface roughness [16,42-46]. However, interesting fabrication solutions [15,47] and thermal oxidation [48] have been proposed in order to reduce scattering losses. Furthermore, SOI slot waveguide exhibits very good fabrication tolerances [17] and small sizes. A slot waveguide based ring resonator in SOI technology characterized by an architecture similar to that sketched in Fig. 8, has been proposed and experimentally tested [21].
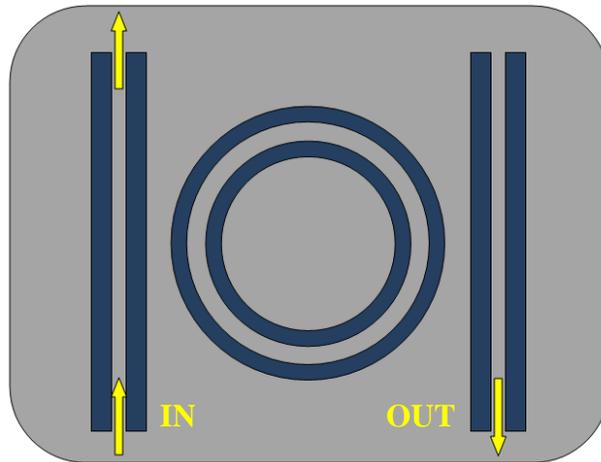

Figure 8. Top view of Si/SiO$_2$ slot-waveguide ring resonator sensor [21].

The sensor has a footprint of only 13 µm×10 µm, which is 150 times smaller than chips made by Si_3N_4/SiO_2 previously described [14]. Moreover, it has been obtained with a low cost, standard SOI wafer with 2 µm thick BOX layer and 220 nm thick upper silicon layer. Authors have numerically optimized the cross section dimension of slot waveguides, in order to maximize the waveguide sensitivity for label-free bio-sensing. Both fabricated input/output bus and ring resonator slot waveguides have silicon wires width of W=268 nm and gap width g=104 nm, while ring radius has been set to R=5 µm.

Experimental measures have shown the homogeneous sensitivity of the slot waveguide based ring resonator to be 298 nm/RIU, that is more than four times larger, compared to 70 nm/RIU of a strip waveguide based ring resonator [49], and 24% larger than that demonstrated in [14]. Furthermore, a LOD as low as 4.2×10^{-6} RIU has been estimated for homogeneous sensing.

A very debated issue, regarding SOI slot waveguide, deals with the filling of the slot region by water, due to capillary and surface tension considerations [16]. Such a consideration is confirmed in [14], where it has been observed that, for a gap width of $g\sim100$ nm, calculated sensitivity stands between theoretical sensitivity of a completely empty slot and theoretical sensitivity of completely filled slot. By this way, the possibility to enlarge the gap width between the two silicon wires has been theoretically investigated in a recent work [50]. It has been found that gap width as high as 200 nm can be successfully obtained in SOI technology, still exhibiting very higher waveguide sensitivities than that obtained with Si_3N_4/SiO_2 technology. The enlargement of the gap width has been

also demonstrated [50] to relax sensibly the fabrication tolerances of the sensor. However, a gap width of 100 nm still enables the sensor to reach ultra-high sensitivity.

Furthermore, the SOI slot waveguide sensor proposed in [14] has been demonstrated to work well for surface sensing purpose, too. In fact, surface chemistry for selective label-free sensing of proteins has been applied, for the first time, inside a 100 nm-wide slot region. The saturation condition has been reached for avidin concentration larger than 10 μg/ml, with a saturation resonance wavelength shift of 2.2 nm, that is 3.5 times more than the shift obtained for a conventional waveguide-based sensor [49]. It has been shown that the measured wavelength shift lies between the two theoretical values calculated for completely filled and completely empty slot region, respectively. By this way, wide improvements are expected with an optimized cross section, involving wider gap, larger waveguide sensitivity and better fabrication tolerances.

Recently, SOI slotted ring resonator sensitivity improvement for label-free detection of a variety of antigen–antibody reactions has been proposed [15]. A sensitivity of 10^{-9} g/ml has been predicted with the use of: i) an operative wavelength λ=1.3 μm, in order to reduce water absorption; ii) on-chip temperature compensation able to maintain temperature within ±0.005 K, in order to avoid thermo-optically induced variations of the resonance wavelength, as discussed above for Si_3N_4/SiO_2 slot waveguides; iii) specific adsorption of the bioreceptor protein to the resonator surface, limiting the adsorption on non device regions; iv) improvement of quality factor Q of the ring resonator by smoothing the surface roughness through isotropic chemical dry etching (CDE) with CF_4+O_2 plasma with a high O_2 content ($O_2/CF_4 = 3$).

Slot waveguides realized in SOI technology have been also proved to be very suitable for gas sensing purposes, as demonstrated in [23]. In this work a chip-scale photonic system for room temperature detection of acetylene gas composition and pressure has been proposed, using a slot waveguide ring resonator coupled to a single slot waveguide straight bus. The sensor operates in the spectral window around 1550 nm. The experimentally measured sensitivity of the sensor has been found to be 490 nm/RIU, in good agreement with the theoretically predicted value. Such a result is sensibly higher than sensitivity values found for aqueous solution cladding, being the refractive index of gases typically much lower than liquid solutions. Moreover, the very good agreement between theoretically predicted and experimentally measured sensitivity confirms the complete filling of the slot region by gas, differently from the aforementioned not complete filling in presence of an aqueous solution. In fact, gasses do not exhibit any relevant problems in terms of capillary and surface tension. The LOD reported by authors is of the order of 10^{-4} RIU, which is enough to detect the presence of acetylene at room temperature and atmospheric pressure [23]. However, sensibly lower LODs can be achieved by increasing the ring resonator Q factor, which is only about 5000 in the proposed device.

Another promising solution, in order to fabricate slot waveguide based bio-sensors, is provided by polymeric materials [32,51]. Polymers are cost effective and fabrication process is easy to be performed, but the principal drawback of polymeric materials is their low refractive index. Reduced index contrast between guiding material and cover region obviously implies larger sizes of the waveguide, in order to avoid cut-off condition. Furthermore, according to equation (6), light-analyte interaction in the slot region will result as very weak, due to the poor field discontinuity at the boundary between polymer and cladding. To overcome such a problem, multiple slot waveguides have been proposed in SU8 polymeric material, as sketched in Fig. 9.
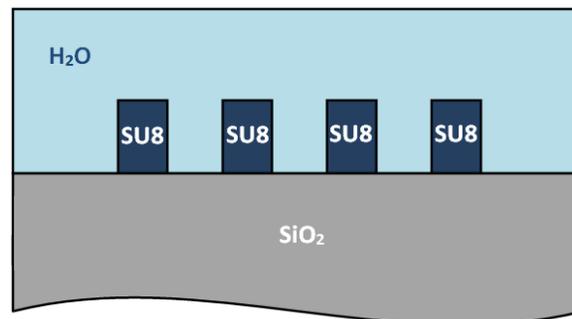

Figure 9. Sketch of SU8/SiO$_2$ multiple slot-waveguide [32].

It is intuitive that, with increasing the number of slots, the waveguide sensitivity should tend to increase. Obviously, the number of slots practically achievable in a slot waveguide is limited by technological considerations, scattering losses, single mode operation and light coupling mechanisms. However, both homogeneous and surface sensing

have been demonstrated by using a reasonable (and optimized) number of slots, i.e. three [51]. In case of homogeneous sensing, sodium chloride (NaCl) solutions in deionized (DI) water with mass concentrations 0 % - 4% has been used to determine the device sensitivity, obtaining the relevant result of 244 nm/RIU. Furthermore, cured SU8 has an hydrophobic nature, making it very suitable for surface sensing purpose. In fact, protein molecules have been immobilized to the waveguide surface through physical adsorption, in order to form a monolayer. Biotin-BSA has been used to characterize the sensor, showing a sensitivity of 1.2×10^{-4} RIU/nm.

3.   DIRECTIONAL COUPLER BASED SENSORS

Ring resonator based sensors are not the unique possible solutions in order to achieve high performance slot waveguide based sensors. Another efficient sensor architecture is represented by the passive directional coupler, as sketched in Fig. 10.
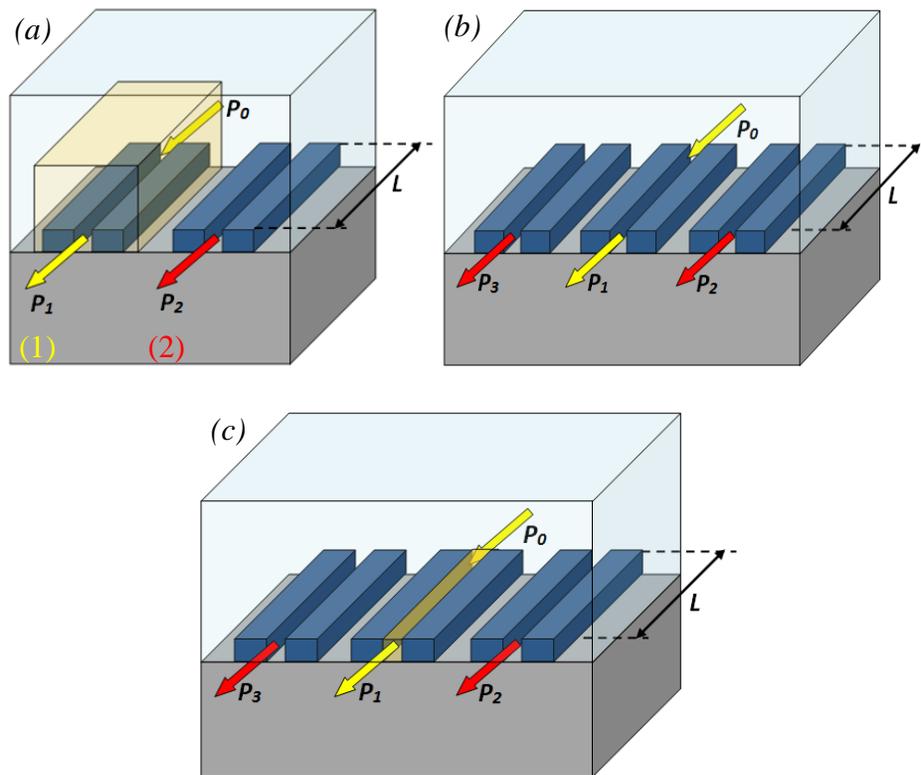

Figure 10. Sketch of single (a) and multiple (b & c) slot-waveguide based directional coupler.

The operative sensing principle used for directional coupler is briefly discussed below. With reference to Fig. 10 (a), light is coupled in the slot waveguide designated as (1), with an input power P_0. Input waveguide is covered by a proper cladding medium characterized by a refractive index n_c^{r}, in order to avoid any interaction between propagating light and analyte, while sensing waveguide (2) interacts with the substance to be detected. After a certain distance ($z = L$), named coupling length, maximum power transfer into waveguide (2) will occur.

Such a device can be effectively modeled by combining the coupled mode theory (CMT) and supermode theory, obtaining an analytical expression for the optical power inside the two waveguides, as a function of all relevant geometrical and optical parameters involved in the design. In particular, assuming both waveguides to be mono-modal, CMT states that optical mode amplitudes, propagating in each waveguide A_1 and A_2 for waveguides (1) and (2), respectively, are related each other by the following coupled differential equations:

$$\begin{cases} \dfrac{\partial A_n}{\partial z} = -j\sum_{m=1}^{2} A_m k_{mn} e^{jk_0\left(n_{eff,n}-n_{eff,m}\right)z} \\ k_{m,n} = \dfrac{\omega}{4}\iint_S \Delta\varepsilon\left[\overline{E}_m(x,y)\cdot\overline{E}_n^*(x,y)\right]dxdy \end{cases} \quad ; \quad n=1,2 \qquad (13)$$

where z is the propagation direction, j is the imaginary unit, $k_0=2\pi/\lambda$ is the free space wavenumber, $n_{eff,1}$ and $n_{eff,2}$ are the effective indices of modes propagating in isolated waveguides (1) and (2), respectively, $\overline{E}_m(x,y)$ is the spatial distribution of the electric field in the unperturbed waveguide (m), $\omega=2\pi c/\lambda$, c is the light speed in vacuum, $\Delta\varepsilon$ and S are the dielectric permittivity perturbation and the surface of perturbation, respectively. By solving for the field amplitude A_1 and A_2, it could be easily found that the normalized transmitted powers at the output port of waveguides (1) and (2) are:

$$\begin{aligned} T_1 &= \frac{P_1}{P_0} = \frac{k_{12}k_{21}}{Q^2}\left[\cos(QL)\right]^2 + \frac{\delta^2}{Q^2} \\ T_2 &= \frac{P_2}{P_0} = \frac{k_{12}k_{21}}{Q^2}\left[\sin(QL)\right]^2 \\ \delta &= \frac{\pi}{\lambda}\left(n_{eff,2}-n_{eff,1}\right)+\frac{k_{22}-k_{11}}{2} \\ Q &= \sqrt{k_{12}k_{21}+\delta^2} \end{aligned} \qquad (14)$$

If the waveguides are sufficiently spaced, k_{nn} coefficients tend to vanish, depending on the squared module of the evanescent mode field integrated on the perturbation area, so equations (14) can be simplified. Furthermore, according to the supermode theory, Q parameter can be conveniently calculated as:

$$Q = \frac{\pi}{\lambda}\left(n_{eff,S}-n_{eff,A}\right) \qquad (15)$$

where $n_{eff,S}$ and $n_{eff,A}$ are the effective mode indices of symmetric and antisymmetric supermodes of the whole structure, respectively. Since both Q and δ depend on the cover medium refractive index (n_c), the power detected at the output of the two waveguides will vary, too, according with equations (14). Homogeneous sensitivity can be therefore defined as:

$$S = \left.\frac{\partial T_1}{\partial n_c}\right|_{n_c=n_c^0} \qquad (16)$$

where T_1 is the normalized power at the output of waveguide (1), n_c is the refractive index of the cladding medium covering waveguide (2), and n_{c0} is the value of n_c in absence of the substance to be detected.

A theoretical analysis of a SOI slot waveguide directional coupler sensor has been performed in [24], oriented to glucose concentration detection in an aqueous solution. In this work, authors propose the use of Teflon as a cover medium for waveguide (1), due to its very poor index difference with respect to water refractive index (n_c^r-n_c^0~0.02 [24]). Overall sensitivity defined by equation (16) obviously depends on both waveguide sensitivity (defined in equation (1)) and device length. In particular, overall sensitivity S exhibits a periodic behavior with respect to L, according to equations (14),(15),(16), and relative maxima have been found to increase with increasing L. The length of the directional coupler has been fixed to 400 μm, as an appropriate trade-off between coupler sensitivity and device footprint. Theoretically estimated sensitivity of the sensor is $S = 500$, simultaneously exhibiting the relevant LOD of ~10^{-5} (0.1 g/L minimum detectable glucose concentration). Another slot directional coupler sensor has been proposed in [52], involving three SOI coupled slot waveguides. Differently from [24], in this work the entire structure is covered by the chemical solution to be analyzed, so the parameter δ in equations (14) can be reasonably assumed to vanish. Such a consideration leads to an equivalence between Q and coupling coefficients (all

equal to k), which varies depending on the concentration of analyte dissolved in the cladding aqueous solution. The normalized device transmittance has been found to vary periodically with respect to the analyte refractive index, so it is needed to optimize the sensor geometry in order to bias the sensor at the maximum slope point. Proposed device has length L=1607 μm and exhibits a sensitivity of S= -172 RIU^{-1} in the bias point of negative slope (around n_c=1.34), corresponding to the detection of glucose in an aqueous solution. Furthermore, the same sensor shows a still relevant sensitivity of S=155 RIU^{-1} in the bias point with positive slope, around n_c=1.36, whose value can be assumed for detection of ethanol dispersed in DI water.

An improvement of results obtained in [52] has been achieved in another work [53]. Authors adopted a basic structure similar to the previous one, however this time the gap region of the center slot was filled by Teflon. Such a design variation involves a difference in the propagation constants of the unperturbed center waveguide with respect to those of lateral slot waveguides, leading an increased sensitivity. The length of the proposed sensor is L=1247 μm (more compact than that in [52]), while theoretically estimated value of sensitivity is S=285 RIU^{-1}, around n_c=1.3341. The same device has been proved to reach a higher sensitivity, S=645 RIU^{-1} around n_c=1.3636.

In conclusion, photonic sensors based on directional couplers have been theoretically proved by several authors to exhibit high performances. However, they have the drawback of a very large device length, so increasing the device footprint and simultaneously enhancing problems related to scattering losses induced by surface roughness. By this way, a good trade-off between sensitivity and device length needs to be achieved, in order to make such devices a feasible solution for sensing purposes.

4. CANTILEVER BASED SENSORS
Another interesting sensing architecture, proposed in very recent years, concerns with horizontal slot waveguides. Differently from vertical slot waveguides, such a device exhibits its performance if excited by a TM-like polarization, because only the E_y-field component can experience a discontinuity at the boundary between high and low index media.

Compared to vertical slot waveguides, which are usually fabricated by an etching process, horizontal ones can be fabricated by deposition of multiple layers or thermal oxidation, strongly reducing the fabrication constraints related to slot thickness (e.g. lithographic resolution, anisotropic etching). Furthermore, horizontal slot waveguides exhibit very low scattering losses due to the small surface or interface roughness. Propagation losses as low as 6.3 ± 0.2 dB/cm and 7.0 ± 0.2 dB/cm have been experimentally demonstrated for single and multiple SOI horizontal slot waveguides, respectively [54]. An optomechanical sensor based on horizontal slot waveguides has been proposed [55]. The sensor consists of an input straight waveguide, coupled to an horizontal slot-waveguide based disk resonator, as sketched in Fig. 11.
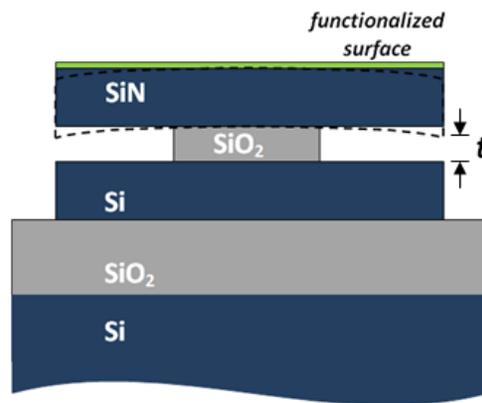

Figure 11. Scheme of a horizontal slot waveguide based disk resonator.

In practice, such a disk acts as a cantilever, and the propagating optical mode effective index has been found to be sensitive to possible variations of the gap thickness t. For example, such a variation could be induced by the absorption of target molecules on the cantilever surface (if properly functionalized). A sensitivity as high as 33 nm^{-1} has been calculated [55], which demonstrates that horizontal slot waveguide can be a very promising solution, compared to the state of the art of cantilever based sensors.

On the other hand, cantilever sensors based on horizontal slot waveguides exhibit some drawbacks. First of all, it is very important to ensure that only particles or molecules involved in sensing detection are responsible for the

variations of *t*. Furthermore, mechanical deformations occurring at each measure, will inevitably reduce the sensor lifetime.

5.   SLOT WAVEGUIDES FOR MOLECULAR TRANSPORT AND NANOPARTICLE HANDLING

The advent of Lab-On-Chips has lead to an even more need of accurate handling of fluid samples, so great efforts have been done by scientific community in order to increase the know-how in the field of optofluidics, which appears to be the most promising solution to join together optical and fluid handling functions.

Nowadays, the state of the art in particle handling consists in the use of optical tweezers, which are based on a highly focused laser beam to provide an attractive or repulsive force (~pN, depending on the refractive index mismatch) to physically hold and move nanoparticles. However, optical tweezers have some intrinsic drawbacks [56], represented by the inability to generate the required forces on small objects over long interaction distances (remote handling), the diffraction limited spot size and the use of free-space optics, which excludes integration with other components and requires high control of alignments.

In recent years, several works [56-59] have shown that evanescent field of an optical mode, propagating into an optical waveguide, is able to generate trapping forces similar to that generated by optical tweezers. This statement leads the possibility to use integrated optical components with microfluidics in order to take a great step forward in the field of optically driven particle transport. Obviously, the use of integrated optics is very attractive in order to reduce cost and size of such a devices, simultaneously enabling the fabrication of extremely compact and robust integrated chips.

Optical waveguide based trapping structures use solid core structures to drive the guided mode (source of the trapping force), but employ a fluid cladding, such that particles suspended in solution can interact with the evanescent mode field outside the waveguide. The propagating mode allows radiation pressure propulsion of particles along the waveguide length. However, for conventional waveguides the evanescent field contains only a small fraction of the total power, generating a weak optical force.

In this context, slot waveguides represent an unique solution, providing a very high optical intensity in a narrow slot region (avoiding any diffraction limit), able to exert the required force on the nanoparticle. The use of SOI slot waveguides has been proposed for trapping and transporting 75-nm dielectric nanoparticles and l-DNA molecules [60]. The two forces involved in the trapping mechanism are sketched in Fig. 12.
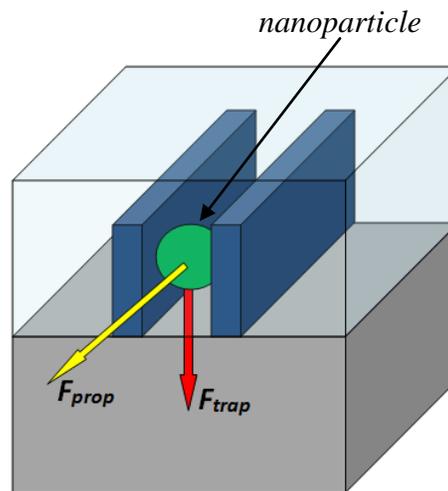

Figure 12. Scheme of the trapping mechanism of nanoparticles with slot waveguides.

The force F_{prop} in Fig. 12 is the radiation pressure force, responsible for optofluidic transport, while F_{trap} is the trapping force holding the nanoparticles within the slot region.

The proposed device operates at the wavelength of $\lambda = 1.55$ μm and it has been experimentally demonstrated to be able to trap polystyrene nanoparticles (refractive index $n = 1.45$) with diameters of 75 and 100 nm in slot waveguides with gap width of 100 and 120 nm, respectively. In all cases, the TE-polarized input optical power coupled into the waveguide is less than 300 mW.

In addition to the ability of trapping nanoscale matter, the proposed device has been demonstrated to be able to transport it optically. This capability leads to very interesting future developments in the field of active nanoassembly and optically driven bioanalytics [61].

Further future improvements of the slot waveguide based optical transport technique may also allow to develop new biomolecular separation mechanisms or new methods of interrogating single molecules for rapid sequencing or direct haplotyping [60,62-63].

In another work, an analysis of optical trapping and transport of sub-100 nm polystyrene and gold nanoparticles in Si/SiO_2 slot waveguides, has been performed [64]. Authors demonstrate as a stable trapping and transport can be achieved for 10 or 20 nm diameter particles, with an increase of trapping stiffness as much as 100 times, compared with the state of the art.

Slot waveguides have been demonstrated to be extremely efficient in sorting micro-particles, too. In fact, an on-chip microparticle passive sorting device has been recently demonstrated [65], showing that the optical force in the vertical direction exerted on small particles (diameter < 1 μm) by the slot waveguide is larger than that achievable by a conventional channel waveguide, while the latter provides a stronger vertical force on large particles (diameter > 1 μm). The in-plane optical force provides a double-well trapping potential for small particles only. The device consists of a 3-dB slot waveguide optical splitter and a conventional channel waveguide. Experiments have been carried out in which small (320 nm diameter) and large (2 μm diameter) particles are brought to the splitter by the channel waveguide. As expected, small particles are transferred to the slot waveguide, while large particles still remain in the channel waveguide. This method is a promising approach, making very simple, effective and automated to sort sub-micron particles, simultaneously matching the requisite of low power consumption (20 mW in author's experiments).

6. OVERALL CONCLUSIONS

Photonic sensors, in particular those based on slot waveguides, represent a real revolution in chemical and biochemical sensing technologies. Some of their most important features can be listed as follows:

- Extremely high selectivity and sensitivity;
- Multi-variable and parallel processing in a chip;
- Wavelength readout (noise and interference immunity);
- Low-cost and high integration with front-end and support electronics systems (silicon, CMOS-compatible processing);
- Real-time processing.

The silicon-on-insulator technology platform allows to integrate Photonics (laser, sensing architecture, photo-detector) and CMOS-Electronics on the same chip in partially monolithic form to constitute the so called Lab-on-a-chip photonic system. Moreover, the refractive index contrast of the Si/SiO2 material system, enables a record reduction in photonic device footprint with ultra-high performance and portability. In all cases, the use of slot waveguides has been proven to be advantageous over conventional waveguides (e.g. photonic wire, rib, ridge waveguide) in terms of sensitivity and potential use in applications requiring the fusion of nanophotonics and nanofluidics. Future work is expected to be focused on the optimization and experimental demonstration of some of the reviewed sensing configurations, extension to other material systems, and development of new sensor architectures based on slot-waveguides for ultra high performance lab-on-chip platforms.

7. ACKNOWLEDGEMENTS

8. REFERENCES
[1]. B.M. Branson, Point-of-Care Rapid Tests for HIV Antibodies, *J. Lab. Med.* **27**, 288-295 (2003).
[2]. L. Gervais, N. de Rooij and E. Delamarche, Microfluidic Chips for Point-of-Care Immunodiagnostics, *Adv. Mater.* **23**, H151-H176 (2011).
[3]. P. Lucas, M.A. Solis, D.L. Coq, C. Juncker, M.R. Riley, J. Collier, D.E. Boesewetter, C. Boussard-Pledel, B. Bureau, Infrared biosensors using hydrophobic chalcogenide fibers sensitized with live cells, *Sensors and Actuators B: Chem.* **119**, 355-362 (2006).
[4]. M. Watanabe, K. Kajikawa, An optical fiber biosensor based on anomalous reflection of gold, *Sensors and Actuators B: Chem.* **89**, 126-130 (2003).
[5]. H. Nguyen-Ngoc, C. Tran-Minh, Fluorescent biosensor using whole cells in an inorganic translucent matrix, *Anal. Chem. Acta* **583**, 161-165 (2007).
[6]. M. Magrisso, O. Etzion, G. Pilch, A. Novodvoretz, G. Perez-Avraham, F. Schlaeffer, R. Marks, Fiber-optic biosensor to assess circulating phagocyte activity by chemiluminescence, *Biosens. Bioelect.* **21**, 1210-1218 (2006).

[7]. S.M. Gautier, L.J. Blum, P.R. Coulet, Fibre-optic biosensor based on luminescence and immobilized enzymes: Microdetermination of sorbitol, ethanol and oxaloacetate, *J. Bioluminesc. Chemiluminesc.* **5**, 57-63 (1990).

[8]. Y. Tian, W. Wang, N. Wu, X. Zou, C. Guthy, X. Wang, A miniature fiber optic refractive index sensor built in a MEMS-based microchannel, *Sensors* **11**, 1078-1087 (2011).

[9]. C.Y. Chao, W. Fung, J. Guo, Polymer Microring Resonators for Biochemical Sensing Applications, *IEEE J. Sel. Top. in Quantum Electron.* **12** , 134-142 (2006).

[10]. R. Jha, A.K. Sharma, Design of a Silicon-based Plasmonic Biosensor Chip for Human Blood-Group Identification, *Sensors and Actuators B* **145**, 200-204 (2010).

[11]. G. T. Kanellos, G. Papaioannou, D. Tsiokos, C. Mitrogiannis, G. Nianios, N. Pleros, Two dimensional Polymer-Embedded Quasi-Distributes FBG Pressure Sensor for Biomedical Applications, *Opt. Express* **18**, 179-186 (2010).

[12]. F. Dell'Olio and V.M.N. Passaro, Optical sensing by optimized silicon slot waveguides, *Opt. Express* **15**, 4977- 4993 (2007).

[13]. V.R. Almeida, Q. Xu, C.A. Barrios, M. Lipson, Guiding and confining light in void nanostructure, *Opt. Lett.* **29**, 1209-1211 (2004).

[14]. C.F. Carlborg, K.B. Gylfason, A. Kazmierczak, F. Dortu, M.J. Banuls Polo, A. Maquieira Catala, G.M. Kresbach, H. Sohlstrom, T. Moh, L. Vivien, J. Popplewell, G. Ronan, C.A. Barrios, G. Stemme and W. van der Wijngaart, A packaged optical slot-waveguide ring resonator sensor array for multiplex label-free assays in labs-on-chips, *Lab Chip* **10**, 281–290 (2010).

[15]. M. Fukuyama, Y. Amemiya, Y. Abe, Y. Onishi, A. Hirowatari, K. Terao, T. Ikeda, A. Kuroda and S. Yokoyama, Sensitivity Improvement of Biosensors Using Si Ring Optical Resonators, *Jap. J. Appl. Phys.* **50**, 04DL11 (2011).

[16]. C.A. Barrios, Optical Slot-Waveguide Based Biochemical Sensors, *Sensors* **9**, 4751-4765 (2009).

[17]. F. De Leonardis, G. Giannoccaro, B. Troia, V.M.N. Passaro and A.G. Perri, Design of Optimized SOI Slot Waveguides for Homogeneous Optical Sensing in Near Infrared, *Advances in Sensors and Interfaces (IWASI)*, *4th IEEE International Workshop on*, 142 - 147 (2011), ISBN 978-1-4577-0622-6.

[18]. H. Sohlström, Highly sensitive lab-on-chip for rapid diagnosis, *SPIE Newsroom* (2010).

[19]. K. B. Gylfason, C. F. Carlborg, A. Kazmierczak, F. Dortu, H. Sohlström, L. Vivien, C. A. Barrios, W. van der Wijngaart, G. Stemme, On-chip temperature compensation in an integrated slot-waveguide ring resonator refractive index sensor array, *Opt. Express* **18**, 3226-3237 (2010).

[20]. T. Claes, W. Bogaerts, and P. Bienstman, Experimental characterization of a silicon photonic biosensor consisting of two cascaded ring resonators based on the Vernier-effect and introduction of a curve fitting method for an improved detection limit, *Opt. Express* **18**, 22747-22761 (2010).

[21]. T. Claes, J. Girones, K. De Vos, P. Bienstman and R. Baets, Label-Free Biosensing With a Slot-Waveguide-Based Ring Resonator in Silicon on Insulator, *IEEE Photonics J.* **1**, 197-204 (2009).

[22]. J. Flueckiger, S.M. Grist, G. Bisra, L. Chrostowski, K.C. Cheung, Cascaded silicon-on-insulator microring resonators for the detection of biomolecules in PDMS microfluidic channels, *Proc. of SPIE*, **7929**, 79290I (2011).

[23]. J.T. Robinson, L. Chen, M. Lipson, On-chip gas detection in silicon optical microcavities, *Opt. Express* **16**, 4296–4301 (2008).

[24]. V.M.N. Passaro, F. Dell'Olio, C. Ciminelli, M.N. Armenise: Efficient chemical sensing by coupled slot SOI waveguides, *Sensors* **9**, 1012–1032 (2009).

[25]. C.A. Barrios, B. Sánchez, K.B. Gylfason, A. Griol, H. Sohlström, M. Holgado and R. Casquel, Demonstration of slot-waveguide structures on silicon nitride / silicon oxide platform, *Opt. Express* **15**, 6846-6856 (2007).

[26]. A.H.J. Yang, S.D. Moore, B.S. Schmidt, M. Klug, M. Lipson and D. Erickson, Optical manipulation of nanoparticles and biomolecules in sub-wavelength slot waveguides, *Nature* **457**, 71-75 (2009).

[27]. C.A. Barrios, M.J. Banuls, V. Gonzalez-Pedro, K.B. Gylfason, B. Sanchez, A. Griol, A. Maquieira, H. Sohlstrom, M. Holgado, R. Casquel, Label-free Optical Biosensing with Slot-Waveguides, *Opt. Lett.* **33**, 708-710 (2008).

[28]. C.A. Barrios, K.B. Gylfason, B. Sánchez, A. Griol, H. Sohlström, M. Holgado, and R. Casquel, Slot-waveguide biochemical sensor, *Opt. Lett.* **32**, 3080-3082 (2007).

[29]. T. Claes, J. Girones, K. De Vos, P. Bienstman, R. Baets, Label-free Biosensing with Silicon-on-Insulator Slotted Racetrack Resonator, *Proc. Symposium IEEE/LEOS Benelux Chapter*, Twente (2008).

[30]. G. Testa, R. Bernini, Slot and Layer-Slot Waveguide in the Visible Spectrum, *J. Lightwave Technol.* **29**, 2979-2984 (2011).

[31]. P. Bettotti, A. Pitanti, E. Rigo, F. De Leonardis, V.M.N. Passaro, L. Pavesi, Modeling of Slot Waveguide Sensors Based on Polymeric Materials, *Sensors* **11**, 7327-7340 (2011).

[32]. H. Sun, A. Chen and L.R. Dalton, Multiple Slot Waveguides for Enhanced Biochemical Sensing, *IEEE/LEOS Int. Conf. on Optical MEMS and Nanophotonics*, 21-22, (2009). ISBN 978-1-4244-2382-8.

[33]. V.M.N. Passaro, B. Troia, F. De Leonardis, Group IV Photonic Slot Structures for Highly Efficient Gas Sensing in mid-IR, *Proc. of IARIA SensorDevices* 2011, 103-108, Nice/Saint Laurent du Var, August 2011, ISBN 978-1-61208-145-8.

[34]. V.M.N. Passaro, B. Troia, F. De Leonardis, Group IV Materials for High Performance Methane Sensing in Novel Slot Optical Waveguides at 2.883 μm and 3.39 μm, *Sensors & Transducers Journal* **137** (2012).

[35]. V.M.N. Passaro, F. Dell'Olio and F. De Leonardis, Ammonia Optical Sensing by Microring Resonators, *Sensors* **7**, 2741-2749 (2007).

[36]. K.R. Hiremath, J. Niegemann and K. Busch, Analysis of light propagation in slotted resonator based systems via coupled-mode theory, *Opt. Express* **19**, 8641-8655 (2011).

[37]. L. Zhou, X. Sun, X. Li and J. Chen, Miniature Microring Resonator Sensor Based on a Hybrid Plasmonic Waveguide, *Sensors* **11**, 6856-6867 (2011).

[38]. J.M. Lee, D.J. Kim, G.H. Kim, O.K. Kwon, K.J. Kim and G. Kim, Controlling temperature dependence of silicon waveguide using slot structure, *Opt. Express* **16**, 1645–1652 (2008).

[39]. G. Maire, L. Vivien, G. Sattler, A. Kaźmierczak, B. Sanchez, K.B. Gylfason, A. Griol, D. Marris-Morini, E. Cassan, D. Giannone, H. Sohlström, D. Hill, High efficiency silicon nitride surface grating couplers, *Opt. Express* **16**, 328-333 (2008).

[40]. C.A. Barrios, M. Holgado, O. Guarneros, K.B. Gylfason, B. Sánchez, R. Casquel, H. Sohlström, Reconfiguration of microring resonators by liquid adhesion, *Appl. Phys. Lett.* **93**, 203114 (2008).

[41]. C.A. Barrios, K.B. Gylfason, B. Sánchez, A. Griol, H. Sohlström, M. Holgado, R. Casquel, Slot-waveguide biochemical sensor, *Opt. Lett*. **32**, 3080–3082 (2007).

[42]. F.P. Payne, J.P.R. Lacey, A theoretical analysis of scattering loss from planar optical waveguides, *Optical and Quantum Electron.* **26**, 977-986 (1994).

[43]. K.K. Lee, D.R. Lim, H.C. Luan, A. Agarwal, J. Foresi and L.C. Kimerling, Effect of size and roughness on light transmission in a Si/SiO2 waveguide: Experiments and model, *Appl. Phys. Lett.* **77**, 1617-1619 (2000).

[44]. Y.A. Vlasov and S.J. McNab, Losses in single-mode silicon-on-insulator strip waveguides and bends, *Opt. Express* **12**, 1622-1631 (2004).

[45]. K.P. Yap, A. Delâge, J. Lapointe, B. Lamontagne, J.H. Schmid, P. Waldron, B.A. Syrett and S. Janz, Correlation of Scattering Loss, Sidewall Roughness and Waveguide Width in Silicon-on-Insulator (SOI) Ridge Waveguides, *J. Lightwave Technol.* **27**, 3999-4008 (2009).

[46]. F. Grillot, L. Vivien, S. Laval, D. Pascal, and E. Cassan Size Influence on the Propagation Loss Induced by Sidewall Roughness in Ultrasmall SOI Waveguides, *IEEE Photon. Tech. Lett.* **16**, 1661-1663 (2004).

[47]. K.K. Lee, D.R. Lim, L.C. Kimerling, J. Shin and F. Cerrina, Fabrication of ultralow-loss Si/SiO2 waveguides by roughness reduction, *Opt Letters* **26**, 1888-1890 (2001).

[48]. Z. Shi, S. Shao, Y. Wang, Improved the Surface Roughness of Silicon Nanophotonic Devices by Thermal Oxidation Method, *Journal of Physics*, *Conf. Ser.* **276,** 012087-7 (2011).

[49]. K. De Vos, I. Bartolozzi, E. Schacht, P. Bienstman, and R. Baets, Silicon-on-insulator microring resonator for sensitive and label-free biosensing, *Opt. Express* **15**, 7610–7615 (2007).

[50]. V.M.N. Passaro and M. La Notte, Optimizing SOI Slot Waveguide Fabrication Tolerances and Strip-Slot Coupling for Very Efficient Optical Sensing, *Sensors* **12**, 2436-2455 (2012).

[51]. H. Sun, A. Chen and L.R. Dalton, Enhanced Evanescent Confinement in Multiple-Slot Waveguides and Its Application in Biochemical Sensing, *IEEE Photonics J.* **1**, 48-57 (2009).

[52]. R.J. McCosker and G.E. Town, Optical chemical sensor using a multi-channel directional coupler with slot waveguides, *Int. Conf. on Photonics* (ICP), 1-5 (2010), ISBN 978-1-4244-7186-7.

[53]. R.J. McCosker and G.E. Town, Multi-channel directional coupler as an evanescent field optical sensor, *Sensors and Actuators B: Chem.* **150**, 417-424 (2010).

[54]. R. Sun, P. Dong, N. Feng, C. Hong, J. Michel, M. Lipson and L. Kimerling, Horizontal single and multiple slot waveguides: optical transmission at λ = 1550nm, *Opt. Express* **15**, 17967-17972 (2007).

[55]. C.A Barrios, Ultrasensitive nanomechanical photonic sensor based on horizontal slot-waveguide resonator, *IEEE Phot. Tech. Lett.* **18**, 2419–2421 (2006).

[56]. A. Yang, Nanophotonic Waveguides For Biomolecular Transport And Particle Control, *Ph.D. Thesis, Cornell University* (2010).

[57]. S. K. Y. Tang, B. T. Mayers, D. V. Vezenov, and G. M. Whitesides, Optical waveguiding using thermal gradients across homogeneous liquids in microfluidic channels, *Appl. Phys. Lett.* **88**, 061112 (2006).

[58]. S. Mandal and D. Erickson, Optofluidic Transport in Liquid Core Waveguiding Structures, *Appl. Phys. Lett.* **90**, 184103 (2007).

[59]. P. Measor, S. Kuehn, E. J. Lunt, B. S. Phillips, A. R. Hawkins, and H. Schmidt, Hollow-core waveguide characterization by optically induced particle transport, *Opt. Lett.* **33**, 672-674 (2008).

[60]. H. J. Yang, S. D. Moore, B. S. Schmidt, M. Klug, M. Lipson, and D. Erickson, Optical manipulation of nanoparticles and biomolecules in sub-wavelength slot waveguides, *Nature* **457**, 71-75 (2009).

[61]. S. J. Hart, A. Terray, T. A. Leski, J. Arnold, and R. Stroud, Discovery of a significant optical chromatographic difference between spores of Bacillus anthracis and its close relative, Bacillus thuringiensis, *Anal. Chem.* **78**, 3221-3225 (2006).

[62]. I. Braslavsky, B. Hebert, E. Kartalov, and S. R. Quake, Sequence information can be obtained from single DNA molecules, *Proc. of the National Academy of Sciences of the United States of America* **100**, 3960-3964 (2003).

[63]. A. T. Woolley, C. Guillemette, C. L. Cheung, D. E. Housman, and C. M. Lieber, Direct haplotyping of kilobase-size DNA using carbon nanotube probes, *Nature Biotechnol.* **18**, 760-763 (2000).

[64]. A. H. J. Yang, T. Lerdsuchatawanich and D. Erickson, Forces and Transport Velocities for a Particle in a Slot Waveguide, *Nano Lett.* **9**, 1182-1188 (2009).

[65]. S. Lin, K.B. Crozier, Microparticle sorting using a slot waveguide splitter, *Proc. of SPIE* (2011).